17 (2023) 100286

Contents lists available at ScienceDirect

International Journal of Thermofluids

journal homepage: www.sciencedirect.com/journal/international-journal-of-thermofluids

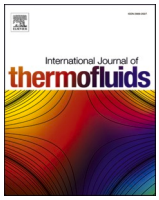

Effects of surface modifications on pool boiling heat transfer with HFE-7100

Genesis Mlakar, Cho-Ning Huang, Chirag Kharangate [*,1]

Department of Mechanical and Aerospace Engineering, Case Western Reserve University, 10900 Euclid Avenue, Cleveland, OH 44106, United States of America

ARTICLE INFO

Keywords:
Pool boiling
Heat transfer
Critical heat flux

ABSTRACT

This study explores pool boiling of HFE-7100 on copper surfaces. The key objective of this study was to examine the effects that surface modifications have on nucleate boiling performance. The surface enhancements studied are roughness, artificial nucleation sites, and a combination of both. Observing roughness between 0.480 μm to 7.564 μm shows that the heat transfer coefficient improves with increasing roughness. Observing hole diameters from 1 mm to 3 mm and hole pitch, or spacing to diameter ratio, from 1.75 to 3.5; a configuration with a hole diameter of 1 mm and pitch of 2.5 provides the best improvement to heat transfer coefficient compared to a bare surface with a roughness of 0.480 μm, while the configuration with a hole diameter of 1 mm and pitch of 3.5 provides worse heat transfer coefficient compared to a bare surface with a roughness of 0.480 μm. Applying a roughness to a hole pattern also improves the heat transfer coefficient with increasing roughness compared to both a bare surface with a roughness of 0.480 μm, as well as to the hole pattern alone. The majority of the surface enhancement modes yield overall improvements in heat transfer coefficient. The introduction of surface enhancement decreases critical heat flux across all samples.

1. Introduction

1.1. Two-phase thermal management

Several advanced electronic systems and devices are seeing an increase in heat rejection requirements that current single-phase cooling schemes are not able to meet satisfactorily. A solution to this problem is using phase-change cooling schemes because they rely on both sensible and latent heat in comparison to single-phase schemes that only utilize sensible heat [1]. Using a two-phase cooling configuration may come with consequential design trades if all shortcomings are not addressed properly. The largest benefit of using two-phase cooling configuration is the significant improvement of heat transfer coefficient (HTC), allowing the rejection of more heat at lower temperatures. As two-phase cooling configurations has been widely used in thermal management, various boiling schemes have been developed and tested in the past. There are numerous studies on pool boiling, the simplest two-phase configuration, which will be discussed in detail in the next section. One of the most widely used two-phase thermal management devices based on pool boiling and recondensation includes a heat pipe [2–5]. Better enhancements are possible with pumped flow boiling. To support this, various flow boiling experiments that investigate the enhancements in HTC and design limits like critical heat flux (CHF) have been performed by the researchers [6–14]. Some other applications such as jet-impingement [15,16] and spray cooling [17] has also been shown to provide good HTC. In recent years, researchers have investigated the utilization of nanofluids as working fluids to show significant improvement in HTC [18–26]. Overall, we see a lot of studies investigating different two-phase configurations all of which can be impacted by the understanding of pool boiling which will be the focus of our study.

1.1.1. Pool boiling studies

Pool boiling on simple surfaces and utilizing a combination of surface enhancement techniques is a continuously expanding and still incomplete field of research, with several papers and experiments attempting to capture this behavior [27]. Simple surface techniques include changing the roughness of the boiling surface which will be discussed in the next section. More complex surface enhancement techniques include surface confinement, porous attachments, microstructures and nanostructures, and hybrid enhancements [28].

* Corresponding author.
E-mail address: chirag.kharangate@case.edu (C. Kharangate).
[1] Website: https://case.edu/engineering/labs/tpftml/

https://doi.org/10.1016/j.ijft.2023.100286

Available online 19 January 2023

Nomenclature

A	Constant
b	Constant
B	Constant
c	Constant
c_p	Specific heat capacity (J/kg-K)
C_{sf}	Constant
D	Diameter (mm)
g	Gravitational acceleration (m/s^2)
h_{fg}	Heat of vaporization (J/kg)
HTC	Heat transfer coefficient (kW/m^2-K)
L	Hole spacing (mm)
L/D	Pitch
k	Thermal conductivity (W/m-K)
M	Molecular weight (g/mol)
m	Constant
N	Nucleation site density (sites/cm^2)
p	Pressure (Pa)
p_r	Relative pressure
Pr	Prandtl Number
q"	Heat flux (kW/m^2)
q	Heat (W)
R	Temperature measurement (°C)
R^2	Coefficient of determination
Ra	Surface roughness (μm)
STD	Standard deviation
T	Temperature (K)
x	Axial coordinate

Greek Symbols

ΔT	Superheat (K)
μ	Dynamic viscosity (kg/m-s)
Φ	Contact angle (radian)
ρ	Density (kg/m^3)

Subscripts

b	Bubble
B	Buoyancy
crit	Critical property
d	Departure property
f	Fluid
fg	Difference between fluid and gas
g	Gas
S	Surface tension
sat	Saturated property

Acronyms

CHF	Critical Heat Flux
DAQ	Data acquisition device
HTC	Heat Transfer Coefficient
MAE	Mean Effective Error
PBM	Pool boiling module
PEEK	Polyether ketone
RTV	Room temperature vulcanized silicone
SC	System controller
SSR	Solid state relay

Porous foams and meshes can be attached just above a boiling surface as a way to introduce more nucleation sites, break up large vapor bubbles, replenish liquid to the boiling surface, and to separate the flow paths of vapor and liquid. Multiple studies show that for thin wire diameters on the order of 0.356 mm, the dimension of the mesh spacing being on the order of the bubble departure diameter, and a spacing between the mesh and boiling surface of around 3 mm yielded optimum results [29]. While HTC increased with the introduction of this mesh, it had an adverse effect on CHF [30]. Metallic foams have different effects on heat transfer based on the number of pores per inch and the expected superheats [31]. With around 30–60 pores per inch, these foams performed better at small superheats; at 60–90 pores per inch, the foams performed better at moderate to larger superheats. Boiling performance can be enhanced further by adjusting the structure of the pores. Another microstructure examined are microchannels in the boiling surface. Often, circular end pockets at the bottom of these channels serve as reentrant cavities, where liquid can more easily replace the departing vapor [32]. The reentry of fluid can also be facilitated by angling the channel. As a result, CHF and HTC both increase with the introduction of this end pocket, and with inclining the channel by up to 50°. Another very common enhancement technique is the use of nanostructures that have 3 classifications, usually as a thin, wiry substrate attached to the surface: Nanotubes, nanowires, and nanofibers. Nanotubes, with diameters ranging from 1 to 100 nm and lengths from 1 to 50 μm, are packed in 300–1432 nm thick coatings where these nanotubes form a random lattice. These nanotubes simulate increased surface roughness and improve fluid wettability. For a silicon substrate covered in these carbon nanotubes, CHF increased by around 50%, and required superheat dropped by over 20 °C [33]. Nanowires, with 10 nm diameters and large length to diameter ratios, are made from either copper or silicon. These nanowire branches are often superhydrophillic and increase nucleation site density. HTC and CHF improved by over 100% for these materials on silicon surfaces [34]. Nanofibers are polymer or copper-plated, electrospun fibers with diameters less than 100 nm. HTC improved by a factor of 3 to 8 for water and ethanol compared to a bare surface, but CHF did not improve [35]. A hybrid enhancement included channels with microporous structures. They showed that for microfins modified with a roughness of 25–32 nm improved CHF in FC-72 by over 2 times compared to regular microfins without any surface roughness or compared to surface roughness alone [36]. However, combining multiple enhancement techniques did not guarantee boiling enhancement greater than the sum of each individual enhancement mode for all tests examined [37]. A comprehensive study on all experiments observed by Liang and Mudawar can be found in the references [28].

1.1.2. *Effect of roughness*

While many of new studies as discussed before investigated novel surface enhancement techniques, early work concentrated on simple roughness and also generation of artificial cavities to enhance boiling performance. The study of surface roughness and its effect on pool boiling is well documented, where higher CHF and HTC and lower superheat are achieved with increasing roughness. The studies examined by Jones indicate that for copper boiling surfaces, the HTC and CHF improve for increasing roughness with FC77 and water as working fluids [38]. They investigated roughness between 0.038–10.0 μm on copper surfaces and showed up to a 100% improvement in HTC with increasing roughness. Their experiment achieved around 25% improvement to CHF for surfaces with roughness up to 2.22 μm but did not run their experiment to CHF for higher roughness samples because of equipment performance limits. Liang and Mudawar's review article corroborated this behavior in several two-phase systems [28]. For roughness between 0.15 and 5 μm for FC-72, hexane, and pentane; and 0.041–2.36 μm for water the CHF increased by up to 100% with increasing roughness [39]. Tests including R-113 with surface roughness introduced by sandblasting gouges in the surface with 15 μm particles also improves CHF and HTC [40]. Jabardo experimented on the effects of roughness with low surface

tension fluids—R-134a and R-123—and with horizontal tubes as the boiling surface [41]. For roughness between 0.07–10.5 μm applied on brass and copper tubes, the HTC and CHF increased with increasing roughness, up to 3.0 μm. With roughness higher than 3.0 μm, the HTC and CHF decreased, with the lowest values of CHF and HTC occurring at 10.5 μm. This indicated that the geometry of the boiling surface itself has an effect on boiling performance—the trends for boiling performance by including roughness on horizontal flat surfaces may not be the same as for horizontal tubes. Fan et al. [42]., Parker and El-Genk [43], Alvarino et al. [44]., looked at pool boiling of HFE-7100 and copper and the effect of roughness on heat transfer. A very recent study on pool boiling was done by Chu et al. [45]. They concluded that the pool boiling heat transfer performance could be enhanced under two scales of structured surfaces, macro-structure surface and micro-structure surface. As shown in the study, macro-structure surface can eliminate the boiling lag and micro-structure can improve the bubble departure diameter, vaporization core density, and critical heat flux. It was observed that the reason for the heat transfer performance enhancement caused by macro-structure surface was due to the increase of the heating area while the micro-structure surface improved the performance by introducing more nucleation sites.

1.1.3. Effect of hole pattern

The act of drilling artificial cavities into the boiling surface has been studied for common liquids such as water. An experiment by Seo et al. shows that the introduction of a hole pattern improved CHF and HTC in deionized water and copper boiling surface systems [46]. The hole patterns they studied varied number of holes and hole diameter. They compared their experimental data to a model using CFD, rather than using a correlation and found enhancements to CHF by over 30% and HTC by up to 26% with required superheat remaining relatively consistent. Das et al. performed an experiment with deionized water on a cylindrical copper surface and a hole pattern of 600 μm diameter holes and spacing of 10 mm [47]. They also covered the bare surface with a screen, so that the holes were the only mode of heat rejection. For this experiment, the CHF increased by over a factor of 3 and the required superheat to achieve CHF decreased by around 5 C°.

The shortcomings in most papers observed is that the coupled effects that diameter, spacing, and hole depth have on pool boiling are not considered. Most studies in literature only look at either one set of chosen hole pattern geometry, or only track the effectiveness that the geometry had on heat transfer by comparing it to a plain surface. Zhang and Shoji observed the effect of pitch, or spacing to bubble diameter ratio, on bubble departure frequency [48]. Their experimental data for water showed that average bubble departure frequency is a local maximum at a pitch of 2.5 and local minimum at 1.75 and absolute minimum of 3.5. Kant and Weber determined that hole depth has an impact on the stability of bubble development [49]. They determined that there are minimum and maximum depth to diameter ratios in which bubble growth is stable. For water, the permissible depth to diameter ratios lay between 0.81 and 1.17, and for isopropanol between 0.83 and 2.28—for ratios that are lower or higher than these ranges, the nucleation site deactivated and bubble growth halted. A paper by Dong et al. performed a comprehensive study of ethanol and silicon wafers with hole patterns of varying diameters and spacing [50]. They observed the behavior on heat transfer performance with changes in hole pattern spacing and diameter. With spacing kept constant, the heat transfer performance increased to a maximum and then decreased compared to a bare surface. With spacing and diameter set equal to each other, the heat transfer performance increased as the diameter and spacing decreased. All augmented samples performed better than a bare surface. The experimental data in Zhang and Shoji, Kant and Weber, and Dong et al. does shed light on the behavior that these parameters have on boiling performance, and these parameters can be controlled in the boiling surface rather than be chosen without justification. Additionally, in most of the papers studied, the surface roughness of the sample not affected by the hole pattern is not always documented—the effect that the surface roughness has on boiling performance is not considered in these studies, as the bare surface can still contribute to heat transfer alongside the hole pattern.

1.2. Objective of study

The objectives of this study are to assess the effects on pool boiling performance of surface engineering with roughness and hole patterns on a copper boiling surface. The working fluid used for the experiment is HFE-7100, a refrigerant manufactured by NOVEC. HFE-7100 is a dielectric, nonflammable, perfluourinated, and low surface tension refrigerant with low toxicity and favorable environmental properties. This fluid is gaining more popularity for use in heat transfer applications including for pool boiling configurations. There are very few research studies thoroughly investigating the combined effect of hole patterns geometries and roughness on pool boiling. In this study, we will first capture the effect of roughnesses on HTC and CHF during pool boiling. Then, we will investigate the effect hole pattern geometry on pool boiling, by adjusting the size, spacing, and number of holes on the surface. Finally, the combined effect of roughness and hole patterns will be uncovered. Overall, we plan to address the shortcomings in the past works by performing a thorough investigation they reveal the effects of roughness alone, the effect of hole patterns with a smooth surface, and the effect of combining the two techniques of roughness and hole patterns on HTC and CHF performance.

2. Experimental setup and procedure

2.1. Pool boiling module

In this study, experiments are conducted on the Pool Boiling Module (PBM). Fig. 1 shows a schematic of the PBM and its components. The PBM allows for the working fluid, HFE-7100, to be maintained at a desired temperature and also allows for modularity in test samples because of a detachable sample assembly design. The PBM reservoir has an interior volume of 20 cm x 20 cm x 20 cm, capable of holding 8 liters of working fluid. Three side walls are made of polycarbonate walls to provide visibility of the experiment. All the surfaces except for the lid are joined on their sides with a 3 M DP8010NS plastic adhesive and sealed from the inside with a high temperature silicon gasket. The lid is sealed mechanically, with a rubber gasket and 8 bolts. The boiling surface and copper heater are sealed mechanically from underneath the bottom wall, with a 2″ diameter bolt pattern, O-ring, and RTV gasket. The top lid has cutouts where two reflux condensers are affixed that allow for evaporated vapor to re-condense. These reflux condensers have chilled water flowing through the coils, which are cooled by an external water chiller. When the evaporated working fluid rises, it will condense on the coils and drip back into the reservoir. The thermocouples which measure fluid temperature and measure wall superheat are fed outside of the reservoir though another cutout in the lid. The degassing of the working fluid is performed by vigorously boiling the liquid in the test chamber and condensing the evaporated vapor using two reflux condensers on top of the test section for a span of 2 h. The degassed working fluid is heated and maintained by up to four 2000 W cartridge heaters mounted in the side wall, a solid state relay (SSR), and a System Controller (SC). The SC is programmed to read the temperature of the working fluid. If the fluid temperature is below saturation temperature, the SC will turn the SSR on and provide power to the cartridge heaters to heat the working fluid back to saturation temperature. When the fluid temperature reaches saturation temperature, the SC will turn the SSR off and cut power to the cartridge heaters. The SC will cycle on and off to maintain the fluid at saturation temperature.

The boiling surface is separately heated by a heating unit that fastens to the reservoir bottom wall. This heating unit is a 1″ x 1″ x 3″ copper slug that is insulated by a ceramic and a PEEK sleeve. Five 120 W, ¼”

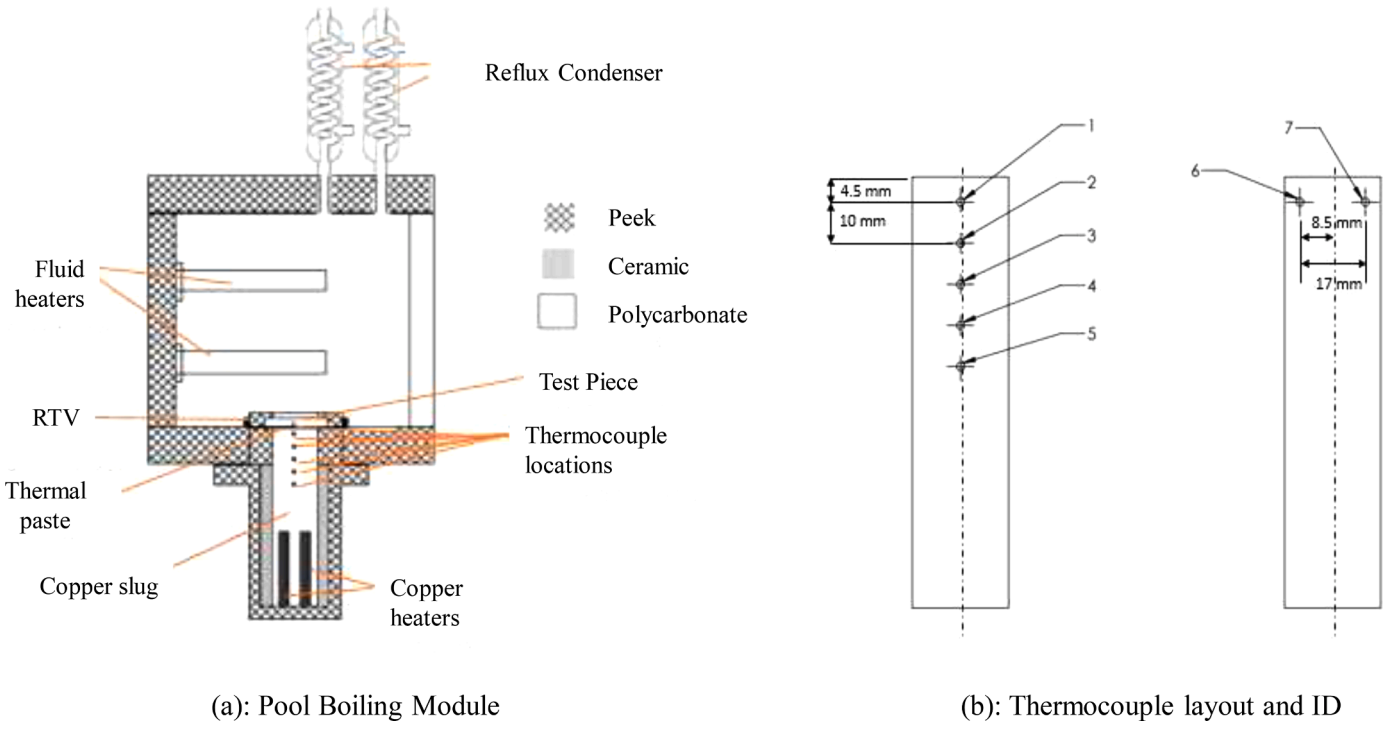

Fig. 1. (a): Pool boiling module. (b): Thermocouple layout and ID.

diameter cartridge heaters are inserted into the bottom of this copper slug to transfer power to the boiling surface. In Fig. 1(b), 7 thermocouples are mounted at the top of the slug and separated vertically by 1 centimeter. These are used for determining heat flux measured by the difference in temperature between adjacent thermocouples and using the equation for conduction.

$$q'' = -k\frac{dT}{dx}$$

The measured heat flux would be the average of the heat fluxes between each thermocouple.

$$q'' = average\left[k\frac{T_i - T_{i+1}}{x}\right]$$

Where i is the current thermocouple ID and $i + 1$ is the adjacent thermocouple ID, and x is the distance between the two thermocouples. The average temperature was used for the top layer of thermocouples.

The following procedure is followed during the individual tests: (1) Increase the power in increments, waiting for the wall superheat and heat flux to reach steady state conditions. (2) Once at a steady state, the data is recorded. (3) Then we move to the next heat flux increment and continue steps (1) and (2) until the CHF is reached. CHF is identified when for a specific heat flux increment, the temperature doesn't reach a steady state but continues to rise continuously. (4) This is followed by decreasing the power in increments, waiting for the wall superheat and heat flux to reach steady state conditions. (5) This is followed until we no longer see boiling.

2.2. Uncertainty

T-type thermocouple inserts were used for all temperature measurements in the experiment, for their low error at +/- 1.0 °C and temperature range of up to 370 °C. These errors will propagate into uncertainties in measuring heat flux. The error in a measurement can be defined:

$$STD = \sqrt{STD_i{}^2\left(\frac{dR}{di}\right)^2 + STD_j{}^2\left(\frac{dR}{dj}\right)^2 + \ldots}$$

Where R is the measurement, and i and j are dependent variable.

The uncertainty of the temperature measurement can be found by deriving the thermocouple calibration temperature equation with respect to temperature. The standard deviation of the difference between the calibrated temperature and the measured temperature is used, and the uncertainty of the temperature measurement is:

$$STD_{T,calibrated} = \sqrt{STD_{(Tcalibrated-T)}{}^2\left(\frac{dT_{Calibrated}}{dT}\right)^2}$$

The uncertainty of the thermocouple measurements is provided in Table 1. IDs 1 – 10 are 1/8″ thick thermocouples used in the PBM and boiling surface heater, and IDs 11 – 20 are 1/16″ thick thermocouples used in the test samples.

Table 1
Thermocouple uncertainty.

Thermocouple	$STD_{(Tcalibrated-T)}$ (K)	Minimum error (K)	Maximum error (K)
T1	0.100	0.101	0.100
T2	0.121	0.122	0.126
T3	0.171	0.172	0.178
T4	0.164	0.163	0.169
T5	0.171	0.171	0.178
T6	0.157	0.156	0.161
T7	0.171	0.170	0.175
T11	0.107	0.104	0.112
T12	0.146	0.143	0.183
T13	0.176	0.173	0.184
T14	0.192	0.186	0.198
T15	0.146	0.142	0.147
T16	0.184	0.178	0.181
T17	0.223	0.216	0.229
T18	0.138	0.134	0.133
T19	0.161	0.156	0.169
T20	0.123	0.120	0.127

For measuring heat flux, the uncertainty can be found from:

$$STD_{q''} = \sqrt{STD_{T_i}{}^2\left(\frac{dq''}{dT_i}\right)^2 + STD_{T_j}{}^2\left(\frac{dq''}{dT_j}\right)^2 + \ldots}$$

Where i and j are thermocouple IDs, and:

$$\frac{dq''}{dT_1} = \frac{1}{2}k\left(-\frac{1}{3x_{5-2}}\right)$$

$$\frac{dq''}{dT_2} = \frac{1}{2}k\left(\frac{1}{x_{2-1}} - \frac{1}{x_{5-2}}\right)$$

$$\frac{dq''}{dT_5} = \frac{1}{2}k\left(\frac{1}{x_{5-2}}\right)$$

$$\frac{dq''}{dT_6} = \frac{1}{2}k\left(-\frac{1}{3x_{2-1}}\right)$$

$$\frac{dq''}{dT_7} = \frac{1}{2}k\left(-\frac{1}{3x_{2-1}}\right)$$

The value for the uncertainty in heat flux is 37 kW/m^2.

2.3. Test samples

For this experiment, the samples are manufactured on 1″ x 1″ x 1/8″ copper plates. For each sample, on the underside is a 1/16″ groove to place a thermocouple to record wall temperature at the center of the sample. This sample is attached to the top of the heating unit by a thermally conductive adhesive and further compressed by a PEEK cover and gasket subassembly with a cut-out for the fluid to have access to the boiling surface. Multiple samples were made with the intent to apply different combinations of surface augmentations: roughness (Sample set A), hole patterns (Sample set B), and a combination of roughness and holes (Sample set C). Individual sample nomenclature is described in Table 2. Sample set A are the samples with differing surface roughness generated through sanding of the test surface. Sandpaper with grits 40 – 2000 were used to generate these profiles, with the intent to gain *Ra* values of 0.5, 2.5, 4.5, and 7.5 μm. Sample roughness was measured using a profilometer. Sample set B are the samples with hole patterns that were machined with an end mill. Two parameters that are adjusted are the hole diameter, and the hole pitch (ratio of L to D), shown in Fig. 2 (a). To control the parameters of artificially created nucleation sites and observe their effects on heat transfer, the hole pattern diameter, pitch, and depth were controlled. The diameter would be the driving variable to determine pitch and depth. All combinations with hole diameters of 1, 2, and 3 mm; and hole pitches of 1.75, 2.5, 3.5 were made—9 samples in total. The surface roughness of these samples were not altered but were recorded to be between 0.5–1 μm, as a baseline roughness of the surface after machining. Sample set C are the samples with both holes and roughness. All individual samples in set A, B and C with their parameter information is summarized in Table 3. Fig. 2(b) shows the actual photo of sample B-1–2. The corresponding surface roughness measured by a profilometer is shown in Fig. 2(c).

Table 2
Nomenclature for all boiling samples.

Sample	Nomenclature
With Surface Roughness	A-Expected Ra
With Hole Pattern	B-Diameter-Pitch
With Surface Roughness and Hole Pattern	C-Diameter-Pitch-Expected Ra

3. Results and discussion

3.1. Sample set A – roughness

The first set of samples investigated are the plain surface samples with only applied roughness. Fig. 3 plots the heat flux vs. superheat for sample A-25 and shows both the increasing heat flux curve until we see CHF and the decreasing heat flux curve. As we can see from the plot, there exists a hysteresis in the curve between increasing heat flux and decreasing heat flux. This is a common behavior observed when investigating pool boiling surfaces [28]. Various reasons cause hysteresis including a possible change in the actual surface profile during the course of the experiment from oxidation, or the working fluid depositing products of decomposition onto the boiling surface, both of which can unintentionally create more nucleation sites. This results in seemingly improved performance during the phase where heat flux is decreasing. However, an adverse effect can occur where the buildup of oxidation and decomposition products can create layers of increased thermal resistance, and thus require larger superheats. Liang and Mudawar also suspected a “thermal shock” from the transition of natural convection to nucleate boiling is responsible for the hysteresis [28]. Additionally, activated nucleation sites may continue to be activated even when supplied heat flux decreases until the natural convection regime. This behavior of hysteresis was observed across sample types and tests, but the reasons for it are not explored in this study. The uncertainty of heat flux estimation is highest at low heat flux levels. Therefore, we limit using data or drawing any conclusions at extremely low heat fluxes which were generally in single-phase condition with no onset of nucleation (<25 kW/m^2). Going forward, we plan to only discuss in this study the data for the heating regime from the experiments where heat flux is increased until CHF is achieved. The differences between the heating and cooling curves as shown in Fig. 3 are not that significant to warrant new discussions so no results on the cooling regimes will be discussed in the following sections.

For all the samples in set A, Fig. 4(a) plots heat flux vs superheat, and Fig. 4(b) plots the corresponding HTC vs heat flux. In Fig. 4(a), sample A-05 is the rightmost curve, and with increasing roughness each curve shifts to the left, with sample A-75 being the leftmost curve. It is observed that with increasing roughness, the boiling curve shifts to the left, signifying that less superheat is required to reject the same amount of heat. This behavior is consistent with past studies that show roughness reducing the required superheat and increasing the corresponding HTC. As seen in Fig. 4(b), we can see that roughness monotonically increases HTC with A-75 showing the highest mean HTCs between samples. Looking at the local HTC curve, it increases after the onset of nucleate boiling but reaches a local maximum midway through the nucleate boiling regime, and then decreases until CHF is achieved. This suggests an optimal value of HTC which exists for a given surface with controlled heat flux and wall temperature. As observed in Fig. 4(a), the heat flux increases at a decaying rate that can explain why the HTC curve has a downward concavity, rather than being linear. As shown in Fig. 4, while the HTC was seen to increase with increase in roughness, the CHF did not change monotonically with change in roughness. The CHF ranged between 250 and 300 kW/m^2, with smooth surface sample, A-05, seeing the largest CHF, and A-50 seeing the smallest value. Fig. 4 (b) shows that, as heat flux approaches CHF, the increment of required superheat increases while the heat flux increases with decay, which is an identifier that the transition from nucleate boiling to CHF is imminent. The comparison between the mean and maximum HTC for individual roughened samples with the smoothest surface sample A-05 is provided in Table 4.

There is no past study that uses HFE-7100 to investigate the effect of hole patterns geometries during pool boiling. However, the effect of roughness has been investigated in one study by Alvarinor et al. [44]. Their results showed CHF of around 20–30 W/cm^2 and HTC of around 6–10 kW/m^2-K depending on the roughness of the surface under 100 kPa

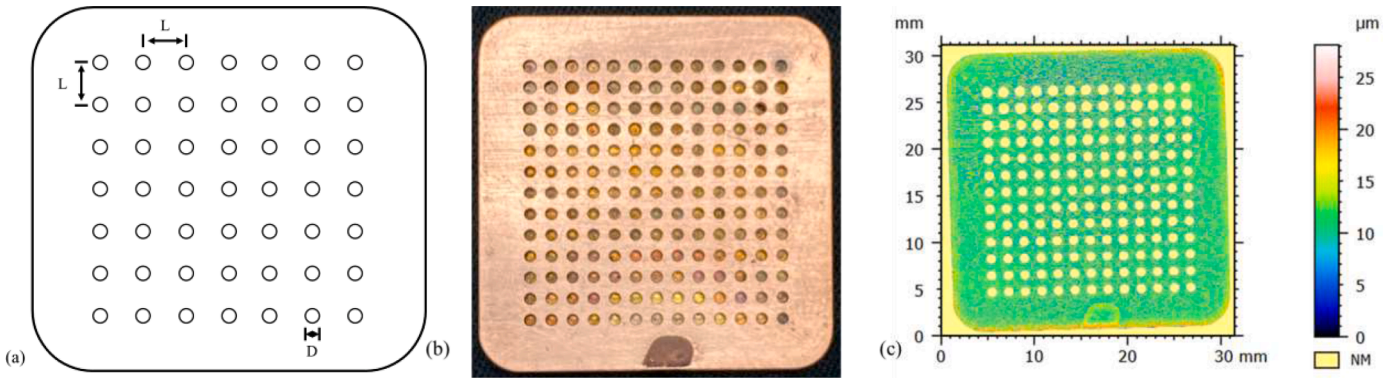

Fig. 2. (a) Diameter and spacing of a hole pattern. (b) Photograph of sample B-1-2. (c) Surface roughness measured using a profilometer for sample B-1-2.

Table 3
Test samples with individual parameter information.

Nomenclature	Diameter-D (mm)	Pitch-L/D	Expected Ra (μm)	Measured Ra (μm)
A-05	N/A	N/A	0.5	0.480
A-25	N/A	N/A	2.5	2.661
A-45	N/A	N/A	4.5	4.416
A-75	N/A	N/A	7.5	7.564
B-1–1	1	1.75	N/A	0.549
B-1–2	1	2.5	N/A	0.577
B-1–3	1	3.5	N/A	0.662
B-2–1	2	1.75	N/A	0.637
B-2–2	2	2.5	N/A	1.066
B-2–3	2	3.5	N/A	1.231
B-3–1	3	1.75	N/A	0.476
B-3–2	3	2.5	N/A	0.397
B-3–3	3	3.5	N/A	0.429
C–1–2–45	1	2.5	4.5	4.764
C–1–3–25	1	3.5	2.5	2.805
C–1–3–45	1	3.5	4.5	4.968
C–1–3–75	1	3.5	7.5	7.307
C–3–1–45	3	1.75	4.5	4.786
C–3–3–45	3	3.5	4.5	4.884

operating pressures. In some other studies utilizing HFE-7100, low roughness (smooth) copper surface were investigated by El-Genk and Bostanci [51] and Priarone [52] and showed CHF around 22 W/cm^2. Overall, these results are close to our data but not the same because no testing condition or operating configuration in those studies is similar to ours.

3.2. Sample set B – holes

The second set of samples observed are the samples with hole patterns as the main enhancement mode. The relationship between heat flux and superheat for sample set B are plotted in Fig. 5. Enhancements of HTC for set B-1,2 and 3 compared with bare surface A-05 are listed in Table 5.

Showed in Table 5, B-1–2 has the best heat transfer performance with around 30% improvement to average HTC and 45% improvement to max HTC. Interestingly, sample B-1–3 does the worst by a detriment of 35%. The samples with diameters of 2 mm (set B-2) and 3 mm (set B-3) have less, but appreciable, sensitivity to the change in pitch. B-2–2 has the best improvement to heat transfer performance, followed by B-2–1. Similarly, with the largest L/D value, B-2–3 do the worse than A-05 by 6.6% on mean HTC. In the samples with diameter of 3 mm samples, B-3–2 still has the best improvement to heat transfer performance.

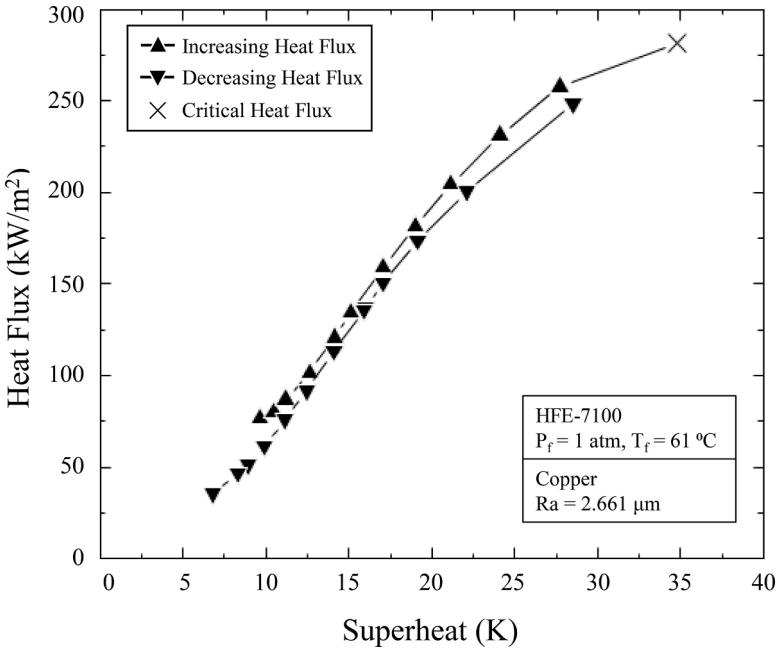

Fig. 3. Heat flux vs superheat for A-25.

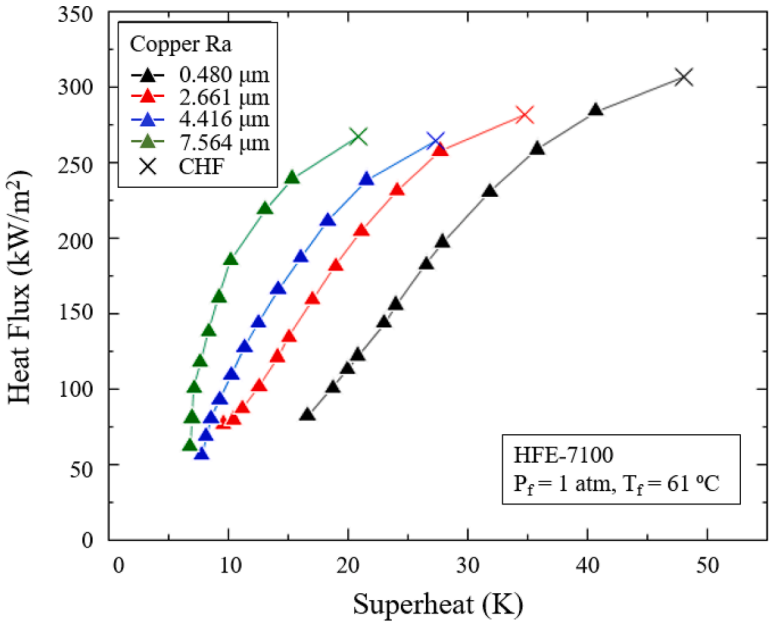

(a): Heat flux vs superheat for sample set A

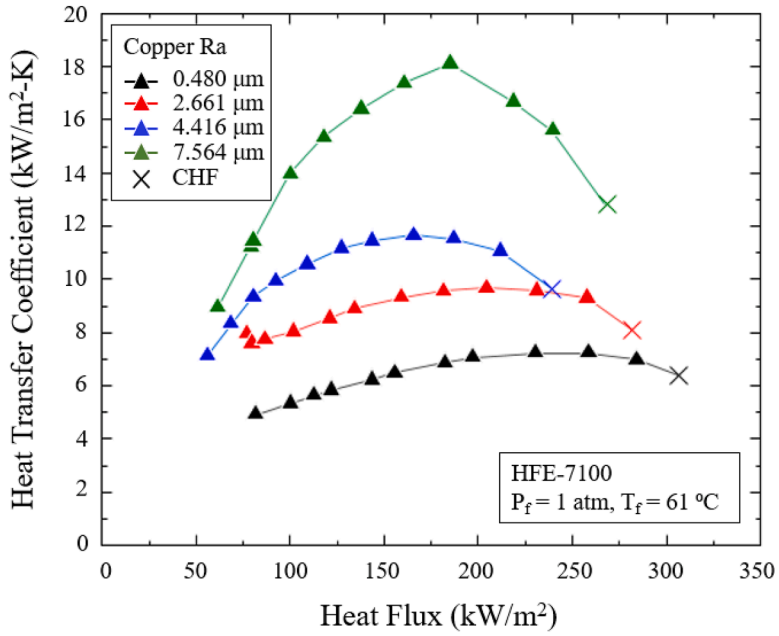

(b): HTC vs heat flux for sample set A

Fig. 4. (a): Heat flux vs superheat for sample set A. (b): HTC vs heat flux for sample set A.

Table 4
HTC enhancement for sample set A.

Sample	HTC_{mean} (kW/m²-K)	HTC_{max} (kW/m²-K)	Enhancement $_{mean}$ (%)	Enhancement $_{max}$ (%)
A-05	5.84	7.23	–	–
A-25	8.08	9.67	27.7	33.7
A-45	9.93	11.66	41.2	61.3
A-75	15.14	18.11	61.4	150.5

However, both B-3–1 and B-3–3 have negative improvement on mean HTC. Out of all the samples, B-1–2 yields the best improvement to HTC. B-1–3 yields the worst detriment to HTC. These combinations of diameter and pitch produce the optimum and worst geometries for improving HTC.

Observed from Fig. 5, the samples with a diameter of 1 mm (set B-1) show the most difference in boiling performance with varying pitch, while the results of different pitches are similar to each other in set B-2 and B-3.

Showed in Fig. 5(a) and 5(b), B-1–2 yields the best HTC and boiling performance out of the others. B-1–3 shows the worst performance and B-1–1 is in between. In terms of CHF, B-1–2 still outperformed from

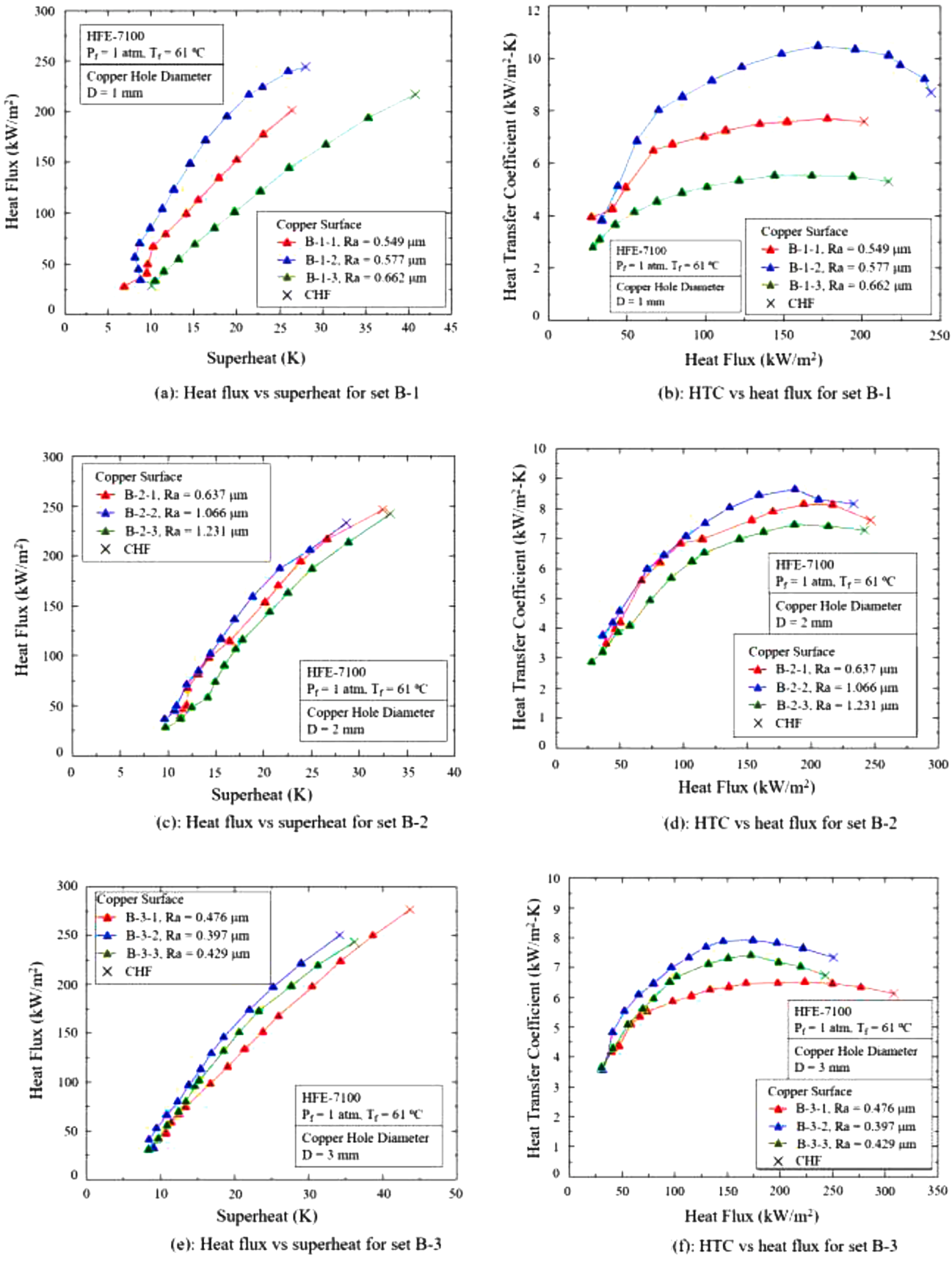

Fig. 5. (a): Heat flux vs superheat for set B-1. (b): HTC vs heat flux for set B-1. (c): Heat flux vs superheat for set B-2. (d): HTC vs heat flux for set B-2. (e): Heat flux vs superheat for set B-3. (f): HTC vs heat flux for set B-3.

Table 5
HTC enhancement for sample set B compared to A-05.

Sample	HTC_{mean} (kW/m^2-K)	HTC_{max} (kW/m^2-K)	Enhancement $_{mean}$ (%)	Enhancement $_{max}$ (%)
A-05	5.84	7.23	–	–
B-1–1	6.37	7.71	8.3	6.6
B-1–2	8.27	10.50	29.4	45.2
B-1–3	4.31	5.53	−35.5	−23.5
B-2–1	5.98	8.14	2.34	12.6
B-2–2	6.35	8.65	8.0	19.6
B-2–3	5.48	7.46	−6.6	3.2
B-3–1	5.39	6.52	−8.3	−9.8
B-3–2	6.32	7.91	7.6	9.4
B-3–3	5.67	7.42	−3.0	2.6

others. However, B-1–1 has the least CHF value while B-1–3 is in between. It is noted that the greatest HTC of each pitch does not happen before reaching CHF. In fact, it can be observed that the greatest HTC happens mostly in the mid part of the boiling curve. The HTC tends to go down slightly before the heat flux reaches CHF. Fig. 5(c) and 5(d) shows the results of set B-2. Similar trend was found as in set B-1. B-2–1 only performs better than B-2–2 at the end of the boiling curve before CHF is reached. Other than that, B-2–2 outperforms the others followed by B-2–1 and B-2–3 shows the worst results. However, the 2 mm diameter samples show less sensitivity to the change of pitch by showing less difference between boiling curves of each pitch than that of set B-1. Greatest CHF was observed in B-2–1 followed by B-2- and then B-2–3. The boiling curves of set B-3 are plotted in Fig. 5(e) and 5(f). Similar to previous two sets, pitch of 2.5 has the best performance. However, it is surprising that B-3–3 has the second best result in set B-3 while B-1–3 and B-2–3 are the worst in their own set. Same as set B-2, the value of CHF decreases as the pitch increases. To sum up, samples with pitch of 2.5 have the best boiling performance among three sets. The samples with pitch of 1.75 tend to perform second best in terms of enhancing boiling performance, and samples with pitch of 3.5 tend to do worst except in set B-3.

In all of the samples in set B, not all of the holes' initiate bubble growth immediately. Bubble activation in all holes occurs after 30 kW/m^2 during the test. Without precision photography and the frequency with which the bubbles depart the surface, it is uncertain how many holes' initiate bubble growth as the test progresses until all sites are activated. This period where not all nucleation sites are activated can explain the odd behavior in the beginning of the boiling curves observed in most of the test cases. Once all nucleation sites are activated, the boiling curve stabilizes into normal behavior expected of the nucleate boiling regime.

3.3. Sample set C – holes and roughness

The last set of samples to be examined are the samples with both surface roughness and hole patterns. Only four samples from set C were first tested to see if the combination of both modes yields significant changes to heat transfer performance. The chosen samples were C-3–1–45, C-3–3–45, C-1–2–45 and C-1–3–45. The samples with diameter of 3 mm yield among the lowest performance in heat transfer, while the samples with diameter of 1 mm yield the highest. Fig. 6 shows the comparison of boiling curve and HTC vs heat flux curves. From Fig. 6(a), the boiling curve shifts upward significantly with rough surface. The heat fluxes increase nearly 50% under same superheat. Fig. 6(b) shows the curves of HTC vs heat flux. Similarly, it is observed that HTCs of C-1–2–45 are much higher HTCs of B-1–2 under same heat flux. Also, C-1–2–45 has much higher CHF than B-1–2 which are around 310 and 250 respectively. The rest of the figures in Fig. 6 show similar trend with Fig. 6(a) and 6(b). A showing of fluctuation of the heat transfer coefficient of C-3–1–45 can be observed in Fig. 6(f). Other than that, the rest of the curves are following the same trend. Table 6 lists the improvements in HTC of all the chosen samples. It is noted that with diameter equal to 1 and L/D equal to 3.5 has the greatest improvement on both mean and max HTC up to almost 150%. Therefore, it can be concluded that surface roughness has huge impact on heat transfer performance in pool boiling.

The introduction of roughness shifts the boiling curves to the left, compared to the same samples with a smoother surface, and shift the HTC curve up and increase HTC significantly—this is similar behavior to the trend in sample set A, where surface roughness improves HTC with increasing roughness. Notably, sample C-1–3–45 yielded the most improvement in HTC compared to sample B-1–3 by nearly 150% when looking at the maximum HTC. The rest of the samples have more modest improvements, from 40 to 90%. For this reason, sample set C-1–3 was tested with the remaining Ra values, with expected Ra from 0.5 to 7.5 μm. The boiling curves for these samples are provided in Fig. 7(a), and the HTC vs heat flux curves in Fig. 7(b). The improvements in HTC are provided in Table 7.

Much like sample set A and the first four samples in this sample set, the boiling curve shifts to the left and HTC increases with increasing roughness, being the most optimal at the highest roughness of 7.307 μm.

4. Correlating with existing correlation forms

4.1. Effect of roughness

A lot of work in the literature shows that experimental data can be easily fitted to the following simple form [38]:

$$HTC = ARa^b q^c.$$

For samples A, we first investigated the data for this general form. As we can see in Fig. 8(a), while the empirical constants can be estimated, the physical properties of the fluid are not realized within this correlation. From both the MAE and R^2 values, the model fits the data very well, and is the most accurate predictor of HTC out of the correlations explored. This is also shown visually in Fig. 8(a), where almost all of the model predictions are within 30% of the data. However, because there is little significance granted to the physical properties of the fluid, these empirical constants only apply to this range of surface roughness, and for the boiling surface and working fluid combination of copper and HFE-7100.

Another well-known correlation is Rohsenow's early model [53] which is described as follows:

$$q_R'' = \mu_l h_{fg}\left(\frac{g(\rho_f-\rho_g)}{\sigma}\right)^{\frac{1}{2}}\left(\frac{c_p\Delta T_s}{C_{sf}h_{fg}\mathrm{Pr}_l^{\,s}}\right)^{\frac{1}{r}}.$$

To determine the empirical constants, the correlation must be fit to the experimental data. Because these constants are dependent on the surface material and working fluid, each experiment must be run and individually fitted. The value of r was fitted to be around 0.33 regardless of the working fluid and boiling surface, which produces curves that are proportional to ΔT^3, which is expected in the nucleate boiling regime. The empirical constant C_{sf} is a modifier dependent on the surface preparation, while the constant s is representative of the fluid's behavior. Jabardo et al. [54]. developed a relationship for C_{sf} that is independent of the fluid and surface material and only dependent on the reduced pressure and surface roughness.

$$C_{sf} = 1.3\{[0.0064\ln(\mathrm{Ra}) - 0.00188]\mathrm{p_r} - 0.00320\ln(\mathrm{Ra}) + 0.0110\},$$

where

$$p_r = \frac{p_g}{p_{crit}}$$

Fig. 8(b) shows that this model is fairly accurate in predicting the value of HTC for the provided Ra measurements, and across most regions of the boiling curve. However, there is more variance in this set of predicted data points compared to the general fit. This can be attributed

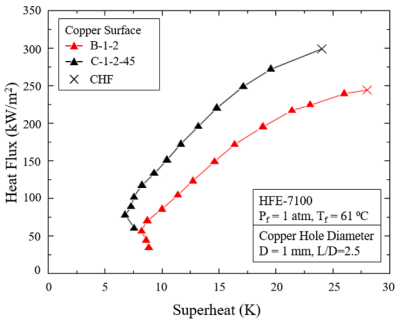

(a): Heat flux vs superheat comparison for B-1-2 and C-1-2-45

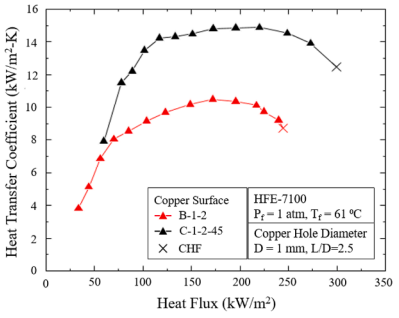

(b): HTC vs heat flux comparison for B-1-2 and C-1-2-45

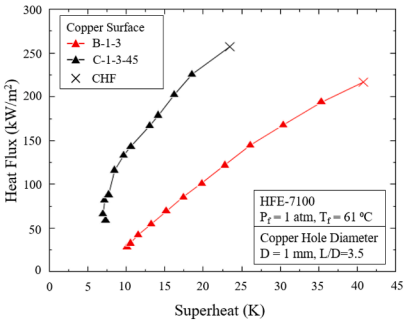

(c): Heat flux vs superheat comparison for B-1-3 and C-1-3-45

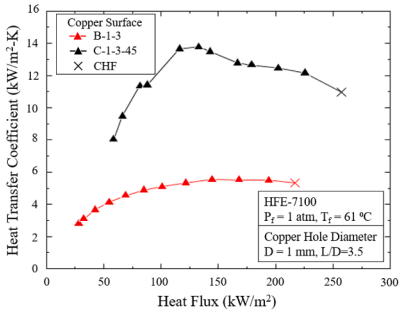

(d): HTC vs heat flux comparison for B-1-3 and C-1-3-45

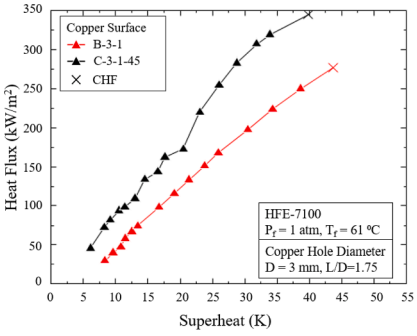

(e): Heat flux vs superheat comparison for B-3-1 and C-3-1-45

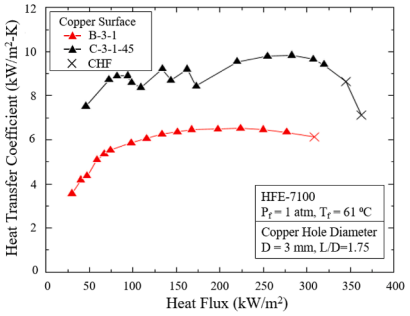

(f): HTC vs heat flux comparison for B-3-1 and C-3-1-45

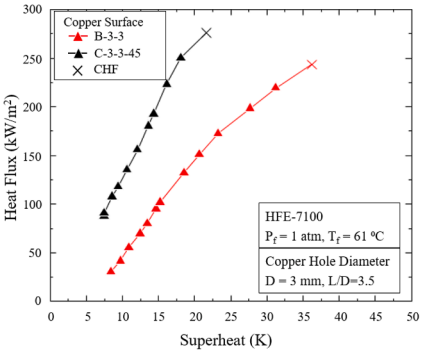

(g): Heat flux vs superheat comparison for B-3-3 and C-3-3-45

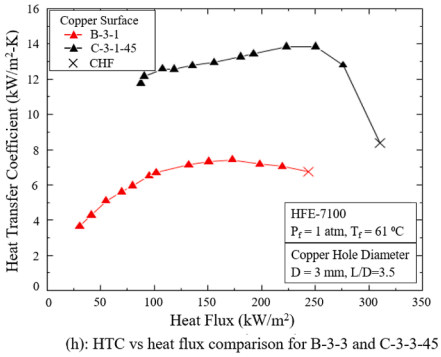

(h): HTC vs heat flux comparison for B-3-3 and C-3-3-45

Fig. 6. (a): Heat flux vs superheat comparison for B-1-2 and C-1-2-45 (b): HTC vs heat flux comparison for B-1-2 and C-1-2-45. (c): Heat flux vs superheat comparison for B-1-3 and C-1-3-45. (d): HTC vs heat flux comparison for B-1-3 and C-1–3-45. (e): Heat flux vs superheat comparison for B-3-1 and C-3-1-45. (f): HTC vs heat flux comparison for B-3-1 and C-3-1-45. (g): Heat flux vs superheat comparison for B-3-3 and C-3-3-45. (h): HTC vs heat flux comparison for B-3-3 and C-3-3-45.

Table 6
HTC improvement in selected samples from set C compared to set B.

Sample	HTC $_{mean}$ (kW/m^2-K)	HTC $_{max}$ (kW/m^2-K)	Improvement $_{mean}$ (%)	Improvement $_{max}$ (%)
B-1–2	8.27	10.50	–	–
C–1–2–45	13.48	14.87	38.6	41.9
B-1–3	4.31	5.53	–	–
C–1–3–45	11.75	13.77	63.3	149.0
B-3–1	5.39	6.52	–	–
C–3–1–45	8.95	9.83	39.8	50.8
B-3–3	5.67	7.42	–	–
C–3–3–45	12.39	13.85	54.2	86.7

Table 7
HTC enhancement for selected samples in set C compared to A-05.

Sample	Ra (μm)	HTC $_{mean}$ (kW/m^2-K)	HTC $_{max}$ (kW/m^2-K)	Improvement $_{mean}$ (%)	Improvement $_{max}$ (%)
A-05	0.480	5.84	7.23	–	–
C–1–3–05	0.662	4.31	5.53	−35.5	−23.5
C–1–3–26	2.805	9.91	11.64	41.1	61.0
C–1–3–45	4.968	11.75	13.75	50.3	90.2
C–1–3–75	7.307	14.32	16.22	59.2	124.3

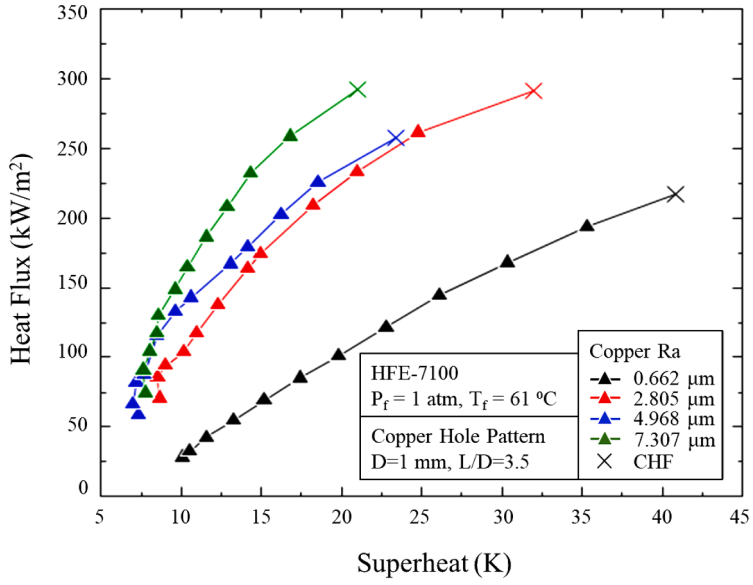

(a): Heat flux vs superheat for sample set C-1-3

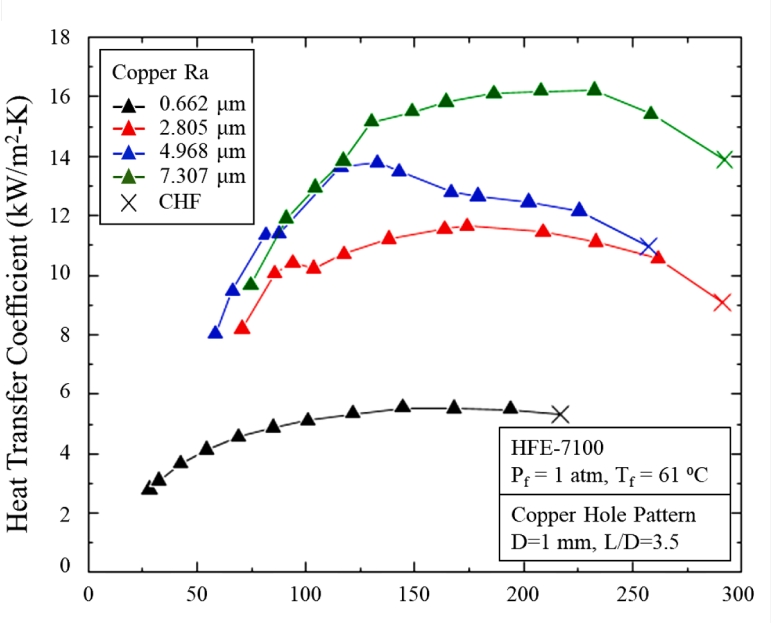

(b): HTC vs heat flux for sample set C-1-3

Fig. 7. (a): Heat flux vs superheat for sample set C-1-3 (b): HTC vs heat flux for sample set C-1-3.

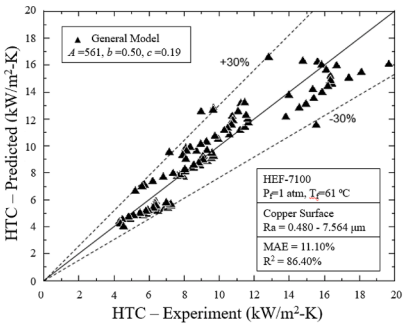

(a): Comparison of predicted data to experimental data for the General model in sample set A

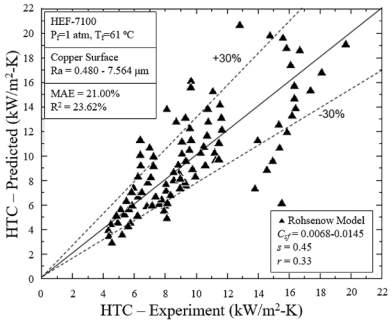

(b): Comparison of predicted data to experimental data for the Rohsenow model in sample set A

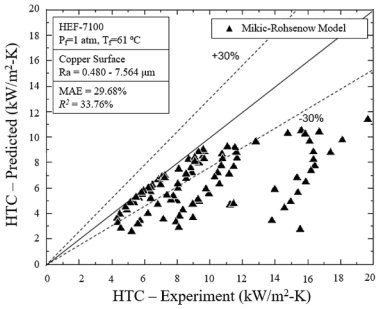

(c): Comparison of predicted data to experimental data for the Mikic-Rohsenow model in sample set A

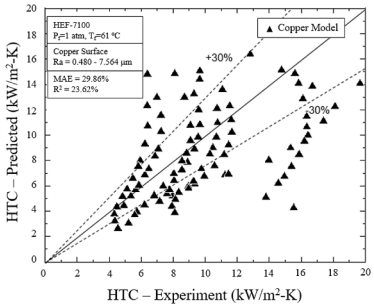

(d): Comparison of predicted data to experimental data for the Copper model in sample set A

Fig. 8. (a): Comparison of predicted data to experimental data for the general model in sample set A. (b): Comparison of predicted data to experimental data for the Rohsenow model in sample set A. (c): Comparison of predicted data to experimental data for the Mikic-Rohsenow model in sample set A. (d): Comparison of predicted data to experimental data for the copper model in sample set A.

to the model not doing well for a few data points. Additionally, it was observed that this model tends to over-predict the HTC when the boiling curve approaches CHF.

The third correlation is by Mikic and Rohsenow [55], who questioned why microlayer evaporation was neglected in several theories even though it is a significant contributor to bubble growth. This model requires knowledge of the bubble departure frequency, bubble departure diameter, and the nucleation site density. Though a surface may feel and look smooth, on the microscale level the surface is populated with several peaks and valleys only micrometers high and deep.

Mikic-Rohsenow model:

$$q_{MR} = Mh_{fg}B\Phi^{m+1}\Delta T^{m+1}$$

This correlation is one of the most robust developed but requires much precision in the measurement of boiling surface parameters, many of which are only feasible with high precision photography. Showing in Fig. 8(c), it is clear that the model poorly predicts the experimental data with an MAE of over 100% and under half of the data following the best-fit line. Specifically, the Mikic-Rohsenow correlation underpredicts most of the data. If this model is assumed to accurately predict heat transfer data, this error must come from the approximations made for bubble departure diameter, frequency, and nucleation site density.

The fourth correlation by Cooper [56] observed that heat transfer coefficient tends to rise with vapor pressure as it approaches critical pressure. Moreover, based on experimental data and the effects that roughness and molecular weight have on HTC, the correlation Cooper arrived at is:

$$HTC_C = 55q''^{0.67}p_r^{\,0.12-0.2\log(Ra)}(-\log p_r)^{-0.55}M^{-0.5}$$

Plotted in Fig. 8(d), this model has more variance than the general fit, with half of the predicted HTC falling within 30% of a perfect fit. The Cooper correlation shows that a model which does not rely on empirical constants can yield preliminary approximations, at the cost of less accuracy compared to a general fit or the Rohsenow correlation.

Overall, this assessment shows us that the HTC correlations whose coefficients were fixed based on other references like Mikic and Rohsenow [55] and Cooper [56] performed worse than the correlations that we developed by generating new coefficients like the general form by Jones et al. [38] and the correlation by Rohsenow [53], which is an expected result due to there being no correlations specifically developed for HFE-7100 on copper boiling surfaces. In addition, we investigated other relevant correlations by Kutateladze [57] and Labuntsov [58] and saw a similar result with MAEs of 33% and 94%, respectively. Because of the new tests we perform with HFE-7100 on a copper surface with varying roughness, no further assessment to validate the data was considered necessary.

4.2. Effect of hole patters

Yamagata and Nishikawa developed a relationship for the performance on heat transfer based on the number of vapor columns attached to the boiling surface [59]. While Yamagata and Nishikawa tested only bare surfaces, Das et al. [60]. [61] successfully applied this correlation to their experiment which studied artificial hole patterns. Yamagata and Nishikawa's model can therefore be applied in cases where the number of vapor columns are analogous to the number of holes with good fidelity. Hara continued on Yamagata and Nishikawa's model and analyzed the thermal boundary layer with Schlieren photography [62]. In the end, the model arrived at is:

$$q''_{Hara} = A\Delta T^b N^c$$

The simplicity of the Yamagata-Nishikawa and Hara correlation, only relying on N and ΔT, make it easy to determine the empirical constants in the correlation for sample set B and C. For each individual

hole diameter or hole pitch, the correlation can be fitted by the least square regression with a set of empirical constants with a value of MAE and R^2. The final empirical constants were decided by optimizing the MAE and the R^2 for both sample sets. The predicted data is modeled in Fig. 9. Fig. 9(a) shows the comparison of the correlation and experimental data in sample set B. The fitted correlation for sample set B is shown as follows.

$$q'' = 4618\,\Delta T^{1.04}\,N^{0.058}$$

There is very little variance in this correlation, and most of the errors which contribute to the MAE and R^2, which are 28.59% and 86.11% respectively, come from the faulty predictions to low heat flux measurements in the boiling curve. Overall, the model shows a good agreement with the sample set B results. However, shown in Fig. 9(b), unlike set B, sample set C fit is more scattered and does a worse job predicting heat flux. The fitted correlation for sample set C is shown below.

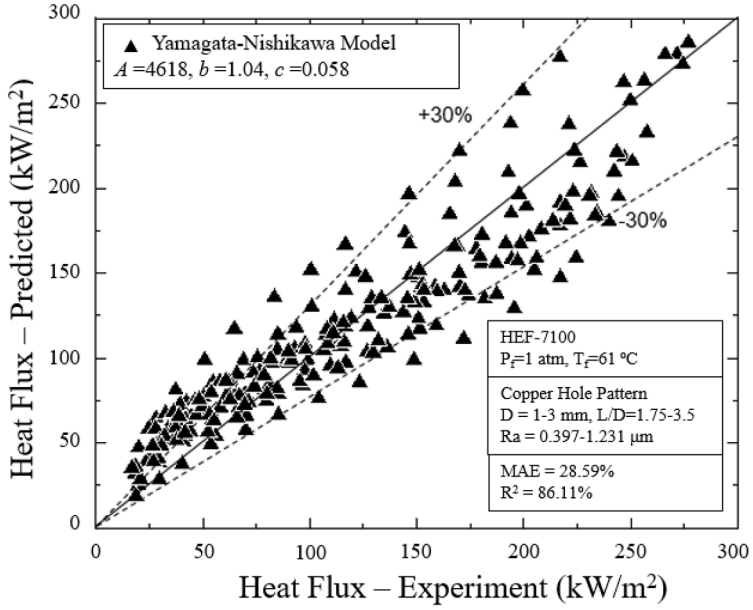

(a): Comparison of predicted data to experimental data for the Yamagata-Nishikawa model in sample set B

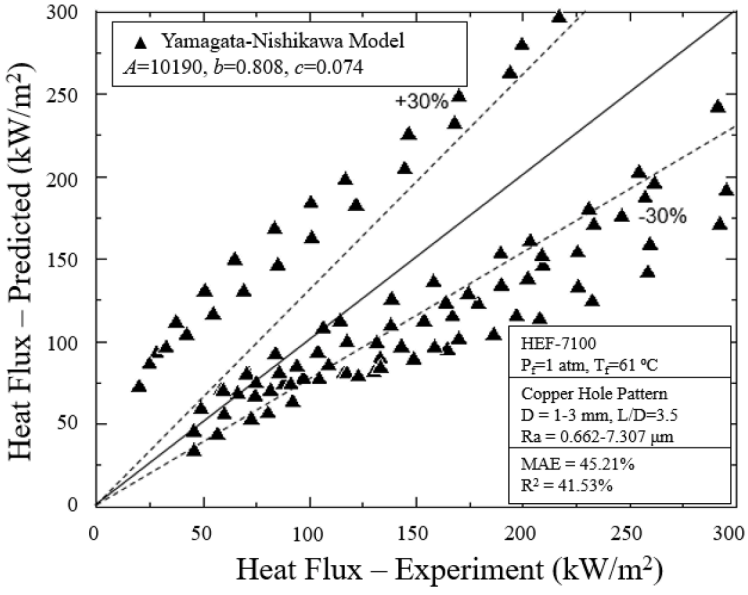

(b): Comparison of predicted data to experimental data for the Yamagata-Nishikawa model in sample set C

Fig. 9. (a): Comparison of predicted data to experimental data for the Yamagata-Nishikawa model in sample set B. (B): Comparison of predicted data to experimental data for the Yamagata-Nishikawa model in sample set C.

$$q'' = 10190\,\Delta T^{0.808}\,N^{0.074}$$

A poor agreement shows with MAE equal to 45.21% and R^2 equal to 41.53%. The reason is that Yamagata-Nishikawa and Hara correlation cannot account for the effects of roughness.

5. Conclusions

This experiment studies the effect of surface engineering has on the heat transfer performance in a HFE-7100 and copper boiling surface pool boiling system. Boiling surface samples have surface roughness (sample set A), artificial nucleation cavities (sample set B), and the combination of both enhancement modes (sample set C). An overall heat transfer coefficient and critical heat flux enhancement in all the sample sets are observed. Key findings from the study are as follows.

(1) For sample set A, the HTC improves by up to 150% for the highest roughness tested of 7.564 μm in comparison to a smooth sample with a roughness of 0.48 μm. The CHF decreases by up to 14% with increasing roughness, but the required superheat to achieve CHF also decreases by up to 27 C°.
(2) For sample set B, the hole patterns with a pitch of 2.5 yields the best improvement to HTC by 10–30%, followed by pitch of 1.75, with a pitch of 3.5 generally decreasing HTC by 8%. CHF did not increase in any of the samples, but the required superheat to achieve CHF decreases by up to 22 C° compared to a bare and smooth surface. The effect that the hole pitch has on HTC is most noticeable on the samples with diameters of 1 mm.
(3) For sample set C, a general improvement to HTC with the combination of a hole pattern and surface roughness, compared to the hole pattern alone as well as to a plain surface was observed. The most improvement to HTC is seen when introducing a surface roughness of 4.968 μm to a hole pattern with diameter of 1 mm and pitch of 3.5, and produces over 60% enhancement to average HTC and 149% enhancement to max HTC compared to the hole pattern alone. The improvement to HTC for the remaining roughness applications onto a hole pattern with diameter of 1 mm and pitch of 3.5 ranges from 30 to 90%. When compared to a bare and smooth surface, sample set C improves average HTC by up to 59% and maximum HTC by up to 124% with increasing roughness. These samples decrease CHF, but all samples decrease the required superheat to achieve CHF by up to 27 C° compared to a bare and smooth surface.
(4) Sample set A is fitted to a general HTC correlation, the Rohsenow correlation, the Mikic-Rohsenow correlation, and the Cooper correlation. Among these correlations, general HTC correlation shows the best agreement. Following is the Rohsenow correlation with 21% of MAE and 23.62% of R2. Both the correlation shows good but not perfect predictions. Mikic-Rohsenow correlation underpredicts the HTC for most of the cases. Last but not least, Copper correlation shows more scattered than general correlation.
(5) Sample sets B and C are fitted to the Yamagata-Nishikawa and Hara model. Sample set B fits very well to the Yamagata-Nishikawa model, except in the beginning of the boiling curve where not all of the nucleation sites are activated and exhibits anomalous behavior in that regime. Sample set C shows poorly agreement due to lacking parameters accounting for surface roughness.

Declaration of Competing Interest

The authors declare that they have no known competing financial interests or personal relationships that could have appeared to influence the work reported in this paper.

Data availability

Data will be made available on request.

Acknowledgements

This project was partly supported by the National Aeronautics and Space Administration (NASA) under grant No. 80NSSC22M0056, the Office of Naval Research (ONR) under Grant Number N00014-21-1-2078, and the National Science Foundation under Grant No. 2138247.

References

[1] I. Mudawar, Two-phase microchannel heat sinks: theory, applications, and limitations, J. Electron. Packag. 133 (2011) 41002–41031.
[2] P.D. Dunn, D. Reay, Heat Pipes, Elsevier, 2012.
[3] A. Faghri, Review and advances in heat pipe science and technology, J. Heat Transf. 134 (2012), https://doi.org/10.1115/1.4007407.
[4] B.D. Marcus, Theory and design of variable conductance heat pipes, (1972).
[5] A. Niro, G.P. Beret-Ta, Boiling regimes in a closed two-phase thermosyphon, n.d. 1972.
[6] C.L. Ong, J.R. Thome, Macro-to-microchannel transition in two-phase flow: part 2–flow boiling heat transfer and critical heat flux, Exp. Therm. Fluid Sci. 35 (2011) 873–886.
[7] C.R. Kharangate, L.E. O'Neill, I. Mudawar, Effects of two-phase inlet quality, mass velocity, flow orientation, and heating perimeter on flow boiling in a rectangular channel: part 1 – two-phase flow and heat transfer results, Int. J. Heat Mass Transf. 103 (2016), https://doi.org/10.1016/j.ijheatmasstransfer.2016.05.060.
[8] C.N. Huang, C.R. Kharangate, A new mechanistic model for predicting flow boiling critical heat flux based on hydrodynamic instabilities, Int. J. Heat Mass Transf. 138 (2019) 1295–1309, https://doi.org/10.1016/J.IJHEATMASSTRANSFER.2019.04.103.
[9] C.N. Huang, C.R. Kharangate, Consolidated model for predicting flow boiling critical heat flux in single-sided and double-sided heated rectangular channels, Int. J. Heat Mass Transf. 160 (2020), 120132, https://doi.org/10.1016/J.IJHEATMASSTRANSFER.2020.120132.
[10] G. Liang, I. Mudawar, Review of pool - boiling enhancement by surface modification, Int. J. Heat Mass Transf. 128 (2019) 892–933, https://doi.org/10.1016/j.ijheatmasstransfer.2018.09.026.
[11] C.R. Kharangate, C. Konishi, I. Mudawar, Consolidated methodology to predicting flow boiling critical heat flux for inclined channels in Earth gravity and for microgravity, Int. J. Heat Mass Transf. 92 (2016), https://doi.org/10.1016/j.ijheatmasstransfer.2015.08.018.
[12] C.L. Ong, J.R. Thome, Flow boiling heat transfer of R134a, R236fa and R245fa in a horizontal 1.030 mm circular channel, Exp. Therm. Fluid Sci. 33 (2009) 651–663, https://doi.org/10.1016/j.expthermflusci.2009.01.002.
[13] H.J. Lee, S.Y. Lee, Heat transfer correlation for boiling flows in small rectangular horizontal channels with low aspect ratios, Int. J. Multiphase Flow 27 (2001) 2043–2062.
[14] L. Tan, C. Chen, X. Dong, Z. Gong, M. Wang, Experimental study on CHF of R134a flow boiling in a horizontal helically-coiled tube near the critical pressure, Exp. Therm. Fluid Sci. 82 (2017) 472–481.
[15] M. Monde, T. Inoue, Critical heat flux in saturated forced convective boiling on a heated disk with multiple impinging jets, J. Heat Transf. 113 (1991) 722–727.
[16] D.C. Wadsworth, I. Mudawar, Enhancement of single-phase heat transfer and critical heat flux from an ultra-high-flux simulated microelectronic heat source to a rectangular impinging jet of dielectric liquid, J. Heat Transf. (Trans. ASME (Am. Soc. Mech. Eng.), Series C);(United States) 114 (1992).
[17] M. Visaria, I. Mudawar, Theoretical and experimental study of the effects of spray inclination on two-phase spray cooling and critical heat flux, Int. J. Heat Mass Transf. 51 (2008) 2398–2410.
[18] Q. Xiong, A. Hajjar, B. Alshuraiaan, M. Izadi, S. Altnji, S.A. Shehzad, State-of-the-art review of nanofluids in solar collectors: a review based on the type of the dispersed nanoparticles, J. Clean. Prod. 310 (2021), 127528, https://doi.org/10.1016/J.JCLEPRO.2021.127528.
[19] Q. Xiong, S. Altnji, T. Tayebi, M. Izadi, A. Hajjar, B. Sundén, L.K.B. Li, A comprehensive review on the application of hybrid nanofluids in solar energy collectors, Sustain. Energy Technol. Assess. 47 (2021), 101341, https://doi.org/10.1016/J.SETA.2021.101341.
[20] M. Izadi, M.M. Shahmardan, A. Behzadmehr, A.M. Rashidi, A. Amrollahi, Modeling of effective thermal conductivity and viscosity of carbon structured nanofluid, Chall. Nano Micro Scale Sci. Technol. 3 (2015) 1–13, https://doi.org/10.7508/tpnms.2015.01.001.
[21] M. Izadi, B. Bastani, M.A. Sheremet, Numerical simulation of thermogravitational energy transport of a hybrid nanoliquid within a porous triangular chamber using the two-phase mixture approach, Adv. Powder Technol. 31 (2020) 2493–2504, https://doi.org/10.1016/J.APT.2020.04.011.
[22] M. Izadi, M. el Haj Assad, Use of nanofluids in solar energy systems, Design and Performance Optimization of Renewable Energy Systems. (2021) 221–250. https://doi.org/10.1016/B978-0-12-821602-6.00017-1.

[23] R. Chand, G.C. Rana, A.K. Hussein, On the onset of thermal instability in a low Prandtl number nanofluid layer in a porous medium, J. Appl. Fluid Mech. 8 (2014) 265–272.
[24] M.S. Kamel, F. Lezsovits, A.K. Hussein, Experimental studies of flow boiling heat transfer by using nanofluids, J. Therm. Anal. Calorim. 138 (2019) 4019–4043.
[25] B. Ali, S. Hussain, Y. Nie, A.K. Hussein, D. Habib, Finite element investigation of Dufour and Soret impacts on MHD rotating flow of Oldroyd-B nanofluid over a stretching sheet with double diffusion Cattaneo Christov heat flux model, Powder Technol. 377 (2021) 439–452.
[26] U. Biswal, S. Chakraverty, B.K. Ojha, A.K. Hussein, Numerical investigation on nanofluid flow between two inclined stretchable walls by optimal homotopy analysis method, J. Comput. Sci. 63 (2022), 101759.
[27] M.M. Mahmoud, T.G. Karayiannis, Pool boiling review: part II – heat transfer enhancement, Therm. Sci. Eng. Prog. 25 (2021), 101023.
[28] G. Liang, I. Mudawar, Review of pool boiling enhancement by surface modification, Int. J. Heat Mass Transf. 128 (2019) 892–933, https://doi.org/10.1016/j.ijheatmasstransfer.2018.09.026, 128.
[29] Y. Zhao, T. Tsuruta, C. Ji, Experimental study of nucleate boiling heat transfer enhancement in a confined space, Exp. Therm. Fluid Sci. 28 (2003) 9–16.
[30] J.W. Liu, D.J. Lee, A. Su, Boiling of methanol and HFE-7100 on heated surface covered with a layer of mesh, Int. J. Heat Mass Transf. 44 (2001) 241–246.
[31] Y. Yang, X. Ji, X. Jinliang, Pool boiling heat transfer on copper foam covers with water as working fluid, Int. J. Therm. Sci. 49 (2010) 1227–1237.
[32] A.K. Das, P.K. Das, P. Saha, Performance of different structured surfaces in nucleate pool- boiling, Appl. Therm. Eng. 29 (2009) 3643–3653.
[33] S. Ujereh, T. Fisher, I. Mudawar, Effects of carbon nanotube arrays on nucleate pool boiling, Int. J. Heat Mass Transf. 50 (2007) 4023–4038, 2.
[34] R. Wen, Q. Li, W. Wang, B. Latour, C.H. Li, C. Li, Y.-.C. Lee, R. Yang, Enhanced bubble nucleation and liquid rewetting for highly efficient boiling heat transfer on two-level hierarchical surfaces with patterned copper nanowire arrays, Nano Energy 38 (2017) 59–65.
[35] R.P. Sahu, S. Sinha-Ray, S. Sinha-Ray, A.L. Yarin, Pool boiling on nano-textured surfaces comprised of electrically-assisted supersonically solution-blown, copper-plated nanofibers: experiments and theory, Int. J. Heat Mass Transf. 87 (2015) 521–535.
[36] H. Honda, H. Takamatsu, J.J. Wei, Enhanced boiling of FC-72 on silicon chips with micro-pin-fins and submicron-scale roughness, J. Heat Transf. 124 (2002) 383–390.
[37] M. Misale, G. Guglielmini, M. Frogheri, A.E. Bergles, FC-72 pool boiling from finned surfaces placed in a narrow channel: preliminary results, Warme- Und Stoffubertragung Zeitschrift 34 (1999) 449–452.
[38] B.J. Jones, J.P. McHale, S. v Garimella, The influence of surface roughness on nucleate pool boiling heat transfer, J. Heat Transf. 131 (2009).
[39] K.N. Rainey, S.M. You, Pool boiling heat transfer from plain and microporous, square pin-finned surfaces in saturated FC-72, J. Heat Transf. 122 (2000) 509–516.
[40] T.M. Anderson, I. Mudawar, Microelectronic cooling by enhanced pool boiling of a dielectric fluorocarbon liquid, J. Heat Transf. 111 (1989) 752–759.
[41] J.M.S. Jabardo, An overview of surface roughness effects on nucleate boiling heat transfer, Open Transp. Phenomena J. 2 (2010) 24–34.
[42] X. Fan, M.M. Mahmoud, A. Ivanov, T.G. Karayiannis, Saturated nucleate boiling with HFE-7100 on a plain smooth copper surface, (2020).
[43] J.L. Parker, Pool Boiling of Dielectric Liquids On Porous Graphite and Extended Copper Surfaces, The University of New Mexico, 2008.
[44] P. Fariñas Alvariño, M.L. Sánchez Simón, M. dos Santos Guzella, J.M. Amado Paz, J.M. Sáiz Jabardo, L. Cabezas Gómez, Experimental investigation of the CHF of HFE-7100 under pool boiling conditions on differently roughened surfaces, Int. J. Heat Mass Transf. 139 (2019) 269–279, https://doi.org/10.1016/J.IJHEATMASSTRANSFER.2019.04.142.
[45] H. Chu, X. Yu, H. Jiang, D. Wang, N. Xu, Progress in enhanced pool boiling heat transfer on macro- and micro-structured surfaces, Int. J. Heat Mass Transf. 200 (2023), https://doi.org/10.1016/j.ijheatmasstransfer.2022.123530.
[46] H. Seo, Y. Lim, H. Shin, I. Cheol, Effects of hole patterns on surface temperature distributions in pool boiling, Int. J. Heat Mass Transf. 120 (2018) 587–596.
[47] A.K. Das, P.K. Das, P. Saha, Nucleate boiling of water from plain and- structured surfaces, Exp. Therm. Fluid Sci. 31 (2007) 967–977.
[48] L. Zhang, M. Shoji, Nucleation site interaction in pool boiling on the artificial surface, Int. J. Heat Mass Transf. 46 (2003) 513–522.
[49] K. Kant, M.E. Weber, Stability of nucleation sites in pool boiling, Exp. Therm. Fluid Sci. 9 (1994) 456–465.
[50] L. Dong, X. Quan, P. Cheng, An experimental investigation of enhanced pool boiling heat transfer from surfaces with micro/nano-structures, Int. J. Heat Mass Transf. 71 (2014) 189–196.
[51] M.S. El-Genk, H. Bostanci, Saturation boiling of HFE-7100 from a copper surface, simulating a microelectronic chip, Int. J. Heat Mass Transf. 46 (2003) 1841–1854, https://doi.org/10.1016/S0017-9310(02)00489-1.
[52] A. Priarone, Effect of surface orientation on nucleate boiling and critical heat flux of dielectric fluids, Int. J. Therm. Sci. 44 (2005) 822–831, https://doi.org/10.1016/J.IJTHERMALSCI.2005.02.014.
[53] W.M. Rohsenow, A method of correlating heat-transfer data for surface boiling of liquids, Trans. ASME 74 (1952) 969–975.
[54] J.M. Jabardo, An overview of surface roughness effects on nucleate boiling heat transfer, Open Conserv. Biol. J. 2 (2010).
[55] B.B. Mikic, W.M. Rohsenow, A new correlation of pool-boiling data including the effect of heating surface characteristics, (1969).
[56] M.G. Cooper, Saturation nucleate pool boiling: a simple correlation, Department of Engineering Science, Oxford University, England. 86 (1984) 785–793.
[57] S.S. Kutateladze, V.M. Borishanskiĭ, A Concise Encyclopedia of Heat Transfer, Pergamon, 1966.
[58] D.A. Labuntsov, Heat transfer problems with nucleate boiling of liquids, Therm. Eng.(USSR)(Engl. Transl.) 19 (9) (1973) 21–28, v.No.Pp.
[59] K. Nishikawa, K. Yamagata, On the correlation of nucleate boiling heat transfer, Int. J. Heat Mass Transf. 1 (1960) 219–235, https://doi.org/10.1016/0017-9310(60)90024-7.
[60] A.K. Das, P.K. Das, P. Saha, Performance of different structured- surfaces in nucleate pool boiling, Appl. Therm. Eng. 29 (2009) 3643–3653.
[61] A.K. Das, P.K. Das, P. Saha, Nucleate boiling of water fro m plain and structured surfaces, Exp. Therm. Fluid Sci. 31 (2007) 967–977.
[62] T. Hara, The mechanism of nucleate boiling heat transfer, Int. J. Heat Mass Transf. 6 (1963) 959–969, https://doi.org/10.1016/0017-9310(63)90051-6.